Pertechnetate/perrhenate-capped Zr/Hf-Dihydroxide Dimers: Elucidating Zr-TcO_4 Co-Mobility in the Nuclear Fuel Cycle

Mohammad Shohel[a], Jenna Bustos[a], Alexander Roseborough[a], and May Nyman*[a]

[a] Dr. M. Shohel, J. Bustos, A. Roseborough, Prof. Dr. M. Nyman
Department of Chemistry, Oregon State University, Corvallis, Oregon 97331, USA.
E-mail: may.nyman@oregonstate.edu

Supporting information for this article is given via a link at the end of the document.

Abstract: Spent nuclear fuel contains heavy element fission products that must be separated for effective reprocessing for a safe and sustainable nuclear fuel cycle. ^{93}Zr and ^{99}Tc are high-yield fission products that co-transport in liquid-liquid extraction processes. Here we seek atomic-level information of this co-extraction process, as well as fundamental knowledge about Zr^{IV} (and Hf^{IV}) aqueous speciation in the presence of topology-directing ligands such as pertechnetate (TcO_4^-) and non-radioactive surrogate perrhenate (ReO_4^-). In this context, we show that the flat tetrameric oxyhydroxyl-cluster $[M^{IV}_4(OH)_8(H_2O)_{16}]^{8+}$ (and related polymers) is dissociated by perrhenate/pertechnetate to yield isostructural dimers, $M_2(OH)_2(XO_4^-)_6(H_2O)_6{\cdot}3H_2O$ (M=Zr/Hf^{IV}; X = Re/Tc^{VII}), elucidated by single-crystal X-ray diffraction. We used these model compounds to understand the pervasive ^{93}Zr-^{99}Tc coextraction with further speciation studies in water, nitric acid, and tetrabutylphosphate (TBP) -kerosene; where the latter two media are relevant to nuclear fuel reprocessing. SAXS (small angle X-ray scattering), compositional evaluation, and where experimentally feasible, ESI-MS (electrospray ionization mass spectrometry) showed that perrhenate/pertechnetate influence Zr/Hf^{IV}-speciation in water. In Zr-XO_4 solvent extraction studies to simulate fuel reprocessing, we provide evidence that TcO_4^- enhances extraction of Zr^{IV}, and compositional analysis of the extracted metal-complexes (Zr-ReO_4 study) is consistent with the crystallized $Zr^{IV}_2(OH)_2(Re^{VII}O_4^-)_6(H_2O)_6$·dimer.

Introduction

The group IV metal cations Zr^{IV} and Hf^{IV} pose similar coordination chemistries and coexist in nature. The nearly identical solid-state chemistry of Hf and Zr is owed to the relativistic effect derived from insertion of the 4f-electrons for Hf. In contrast, their nuclear chemistry is very different. A primary use of Zr is in the nuclear industry. Zr-based alloys are exploited as fuel cladding and matrixes, due to high corrosion resistance and low neutron absorption. Hf is likewise used in the nuclear industry,[1] but for its high neutron absorption behaviour. For nuclear grade Zr, Hf impurities must be as low as possible, and vice versa. Therefore, understanding differences in their solution speciation is crucial for separation processes.[1-2]

Zr/Hf^{IV}-oxocluster chemistry has been in the limelight since 2008 with the discovery of the UiO-66 metal-organic framework (MOF) featuring the $Zr^{IV}_6O_4(OH)_4^{12+}$ node (**Figure 1A**), followed by the Hf-analogue in 2012,[3] and related nodes Zr_8[4] and the M_{12}-dimer of hexamers (M=Zr,Hf).[5] The Zr/Hf-oxocluster MOFs have been exploited in numerous applications[6] including degrading chemical warfare agents,**[7]** capturing radioisotopes,**[8]** CO_2 capture/separation[9], catalysis[10], and selective hydrolysis of peptide bonds for proteomics and biotechnology applications.**[11]**

Controlling Zr/Hf-oxocluster assembly leading to different topologies and nuclearity is equally important to understanding and orchestrating reaction pathways and materials properties in MOF synthesis, as well as parallel applications of the isolated oxoclusters (including Zr/Hf industrial separations).[2, 12] For example, precise control of Hf-oxocluster nuclearity coupled with Hf's high absorption of extreme-UV energy is exploited in nanolithography.[12d] The flat tetramer $M^{IV}_4(OH)_8(H_2O)_{16}^{8+}$ (Zr_4/Hf_4), commonly known and sold as '$MOCl_2xH_2O$' is the simplest Zr/Hf-oxocluster, isolated from solutions with non-coordinating anions (**fig. 1**, centre). It is obtained from HCl solution,[13] more recently with perchlorate as the acid/counteranion;[14] and it demonstrates that hydrolysis reactions of these Lewis acid M^{IV}-cations occur even at very low pH. As a commercially-available and air/water stable solid, it is usually the starting point of assembling a variety Zr/Hf clusters with topologies differentiated by coordinating anions (**figure 1**). Alternative anions have a strong influence on obtained oxocluster topology and nuclearity. Select examples include Zr_6/Hf_6[15] (carboxylates, **fig. 1A**), $Zr_{17/18}$/Hf_{17}[15] [16] and Zr_{70}[17] (sulphate, **fig. 1B**), tetrahedral Zr_4, Zr_{25} [14] and Zr/Hf_6-ring[18] (peroxide and oxalate, **fig. 1C)**, Zr-hydroxide chains (nitrate, **fig. 1D**)[19], and tetrahedral Zr/Hf_4 and Zr_{48} (thiocyanate, **fig. 1E**)[12a]. It has become apparent in recent years that Zr^{IV} exhibits greater coordination lability in water than Hf^{IV}, leading to a more expansive family of polyoxocations, as highlighted in the above list.[20]

In addition to use of the Zr-alloy as cladding or matrix material for nuclear fuel, the ^{235}U fission reaction produces ^{93}Zr as one of the highest yield and longest-lived decay products that exist in spent nuclear fuel (SNF). ^{99}Tc is another high yield and long-lived decay product of ^{235}U fission, and it is a matter of concern due to both its mobility in the environment, volatility as a neutral oxide Tc_2O_7, and its tendency to hamper efficient separations of radionuclides during SNF reprocessing. Specifically, pertechnetate, TcO_4^-, co-extracts with different metal cations including high valence actinides and zirconium. Chemical interactions of Zr with Tc are particularly important; Zr is found to increase undesirable extraction of TcO_4^-, more so than any other metals present in SNF[21]. An additional unrelated motivation to study Zr and Tc co-speciation is both ^{89}Zr and ^{99}Tc are useful medical imaging isotopes.[22]

Several studies have shown that TcO_4^- and its well-known surrogate ReO_4^- can directly ligate actinides, and this phenomenon is possibly a key step for co-extraction.[23] Currently, we are developing the coordination chemistry of ReO_4^-/TcO_4^- with relevant high oxidation state metals (M = Zr^{IV}, Hf^{IV}, Ce^{IV}, Th^{IV},[24] $U^{IV/VI}$, $Pu^{IV/VI}$) to (1) Understand pertechnetate speciation in relevant nuclear industrial waste and contamination settings, and (2) Determine the differentiating effect of this oxoanion on $M^{IV/VI}$-speciation, including Hf and Zr. While no Zr-TcO_4^-/ReO_4^- hybrid molecules have been isolated, the enhanced co-extractability of Zr and Tc suggests formation of a Zr-TcO_4^- complex.[21a] In prior computational and experimental studies, molecular formulae featuring 1:1 and 2:1 TcO_4:Zr plus nitrates and TBP (tributylphosphate) molecules are suggested; i.e. $[Zr^{IV}(NO_3)_4(TcO_4)(TBP)]$ or $[Zr^{IV}(NO_3)_2(TcO_4)_2(TBP)_2]$.[25] However, the structure of these proposed hetero-ligand complexes is unknown.

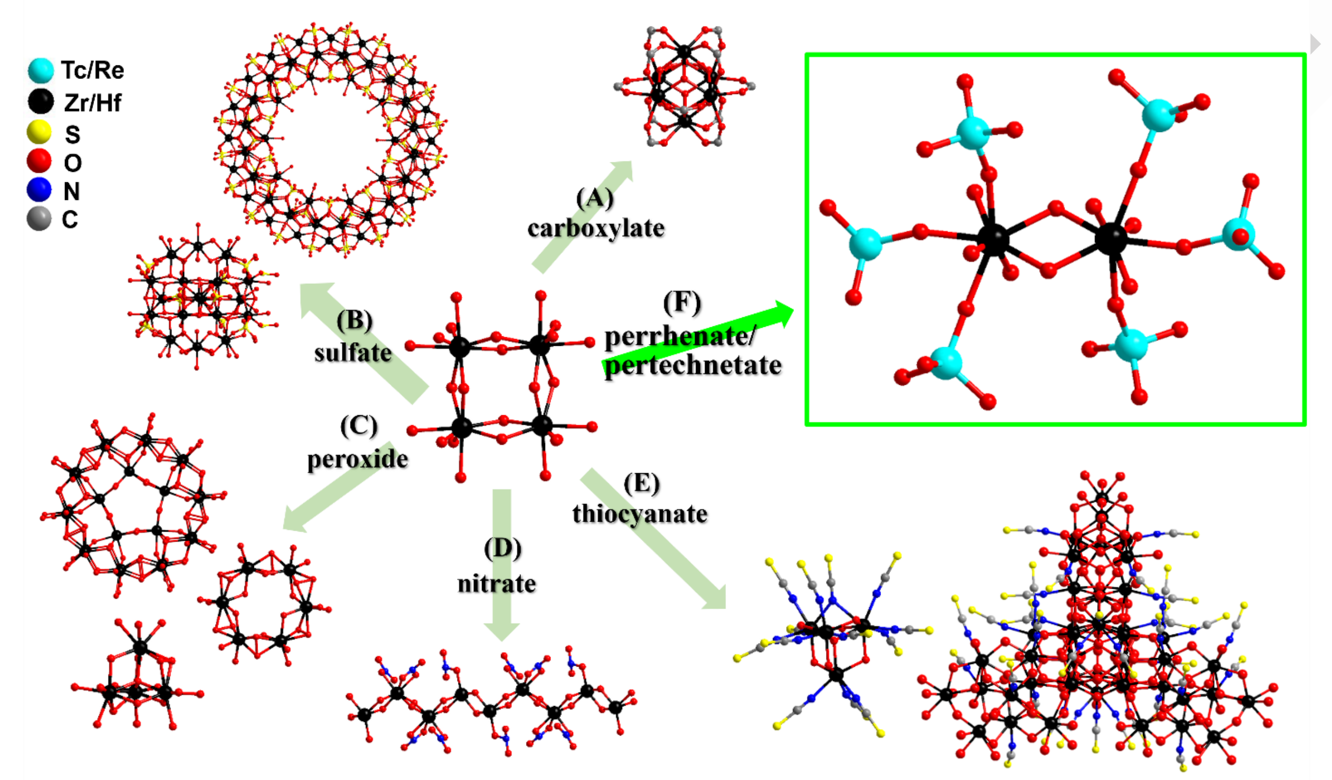

Figure 1. Ball and stick representation of a selection of previously isolated Zr/Hf-oxo molecular clusters starting with the M_4 flat tetramer using different anions (**A - E**). This figure also highlights $M_2(OH)_2(XO_4^-)_6(H_2O)_6{\cdot}3H_2O$ **(M=Zr/Hf^{IV}; X = Re/Tc^{VII})** isolated in the current study with perrhenate/pertechnetate as the anion (**F**).

Here we report the synthesis and structural characterization of four isostructural dimer compounds that illustrate direct ligation of Zr/Hf with perrhenate/pertechnetate, formulated $M_2(OH)_2(XO_4^-)_6(H_2O)_6$ (M= Zr^{IV} or Hf^{IV}; X= Re^{VII} or Tc^{VII}, referred to as **Zr_2Re_6**, **Hf_2Re_6**, **Zr_2Tc_6** and **Hf_2Tc_6**). In addition, we investigated the formation and phase transfer of these compounds in conditions relevant to UREX/PUREX processes (respectively uranium extraction and plutonium uranium reduction extraction).[26] To simulate these industrial processes, we studied the transfer of inorganic molecules from 1M HNO_3 solution into 1M TBP in kerosene. M-XO_4 speciation in water, nitric acid and TBP-kerosene was studied via SAXS (small angle X-ray scattering), and the aqueous solutions were studied via ESI-MS (electrospray ionization mass spectrometry). SAXS shows the perrhenate/pertechnetate stabilizes the Zr_2/Hf_2-dimer in water and interferes with Zr/Hf-polymerization. ESI MS also evidences persistence of the dimers and Zr-ReO_4 complexation in water and organic media. SAXS of Zr-XO_4 (X=Re, Tc) complexes extracted from nitric acid into TBP-kerosene indicates that Zr^{IV}-species alone do not extract extensively, but there is evidence for extraction of polynuclear species for Zr-ReO_4 and Zr-TcO_4, as well for as $HReO_4$ and $HTcO_4$ alone. Compositional analysis of the extracted Zr-ReO_4 indicated presence of both Zr and Re, in the 1:3 ratio, consistent with the **Zr_2Re_6**-dimer. Moreover, **Zr_2Re_6** crystallizes out of the nitric acid solution, evidencing the preferred coordination of perrhenate/pertechnetate, despite the excess of nitrate that can also serve as a capping group (**figure 1D**). These data taken together provide a prospective on Zr/Hf-ReO_4/TcO_4 speciation in water, in conditions relevant to nuclear fuel reprocessing, and the possible role of Zr-pertechnetate bonding in the pervasive co-extraction problem.[21b]

Results and Discussion

Synthesis and solid-state characterization of Zr_2Re_6, Hf_2Re_6, Zr_2Tc_6 and Hf_2Tc_6

Both TcO_4^- and ReO_4^- ligate Zr/Hf^{IV} invariably, splitting the common Zr_4/Hf_4 flat tetramer **(figure 1F)** to yield a dihydroxide-bridged dimer, exemplified in four isostructural compounds determined by single-crystal X-ray diffraction; $M_2(OH)_2(XO_4^-)_6(H_2O)_6$ (M= Zr^{IV} or Hf^{IV}; X= Re^{VII} or Tc^{VII}, referred to later as **Zr_2Re_6, Hf_2Re_6, Zr_2Tc_6** and **Hf_2Tc_6**; see SI for synthesis details). This dimer was recently predicted by computation to be the first step of Zr/Hf-hydrolysis,[27] but not observed in an isolated and soluble form, prior to this current study. The Zr/Hf-dimers (**figure 1F**) were synthesized two ways; 1) By dissolving corresponding Zr/Hf oxyhydroxide in perrhenic/pertechnic acid, or 2) By co-dissolving the corresponding oxychloride salt (Zr_4/Hf_4) with perrhenic/pertechnic acid, followed by slow evaporation to yield crystals (see SI for more details). The experimental details of X-ray structure data collection and refinement, along with selected crystallographic parameters (**Table S1**) are provided in the SI.

All four Zr/Hf-dimer compounds are isostructural, crystallized in the monoclinic space group *C*2/c. The metal centres in the dimers are connected by two μ_2-OH ligands with Zr-OH distances of 2.085(4) Å - 2.169(5) Å and Hf-OH distances of 2.085(5) Å - 2.158(5) Å (**figure 1F**). Each Zr/Hf is additionally coordinated by three XO_4^- (X=Re/Tc^{VII}) and three H_2O, yielding eight-coordinate Zr/Hf and an overall neutral moiety formula of $M_2(OH)_2(XO_4)_6(H_2O)_6$ (M= Zr/Hf^{IV}; X= Re/Tc^{VII}). The Zr-O_{Tc} and Zr-O_{Re} bond lengths are slightly longer than the corresponding Hf-O_{Tc} and Hf-O_{Re} bond lengths (**Table S2**), consistent with the slightly smaller Hf^{IV} radius. Similarly, the M-O_{Tc} bonds are slightly shorter than M-O_{Re} bond distances, corresponding with longer Tc-O bond distances (**Table S2**). In the extended lattice, the dimers are arranged parallel approximately in the (1 0 -1) direction, best viewed down the *b*-axis (**fig. S1**). Lattice water molecules that align along the *c*-direction (three per dimer) are located at hydrogen-bonding distance to the pertechnetate/perrhenate oxygens (~2.6-2.8 Å), giving a complete formula of $M_2(OH)_2(XO_4)_6(H_2O)_6{\cdot}3H_2O$ (M= Zr^{IV} or Hf^{IV}). The dimeric unit of Zr/Hf was observed once prior in an insoluble framework linked by sulphate, obtained from hydrothermal synthesis.[28] The analogous sulphate phase was also identified via PXRD for Pu(IV), Ce(IV),[29] and similar Th(IV) dimers have been isolated multiple times with different capping and bridging anions.[30]

Additional solid-state bulk analysis of Zr_2Re_6 and Hf_2Re_6 includes Scanning Electron Microscopy-Energy Dispersive Spectroscopy (SEM-EDS), Powder X-ray Diffraction (PXRD), Fourier-Transform Infrared Spectroscopy (FT-IR) and Thermogravimetric Analysis (TGA) (see SI for experimental details). For the Tc analogues, characterization was limited to only SEM-EDS due to institutional restrictions, and the inability to separate the dimer phase from impurities (see SI).

Blocky and tabular crystals are observed by SEM analysis of the isolated crystalline materials of all studied compositions (**figure S2- S5**). The metal to oxoanion (M^{IV}/XO_4^-) ratios observed from EDS analysis were between 2.64-3.27 (**Tables S2- S5**), consistent with calculated molecular formula from refined crystal structure. The PXRD pattern of synthesized Zr_2Re_6 and Hf_2Re_6 crystalline materials is similar to the calculated pattern from crystallographic information files (cif, **figure S6**). However, preferred orientation leads to non-ideal matching in the relative peak intensity between simulated and experimental diffraction. In sum, the combined PXRD and EDS suggests the compounds characterized by SCXRD are representative of the bulk solids. Interestingly, all syntheses employing different ratios of X:M (X=Tc,Re; M=Zr,Hf) yielded only the reported dimer phase, highlighting its ubiquity and presumed stability.

The FT-IR spectra of Zr_2Re_6 and Hf_2Re_6 crystals show evidence of hydroxyl and water through a broad O-H stretching peak between 2800-3600 cm^{-1} and a sharp H_2O bending peak in between 1500-1720 cm^{-1} (**fig. S7**)[31]. The characteristic peaks for ReO_4^- υ_1 and υ_3 stretching are observed between 905-930 cm^{-1} and 840-880 cm^{-1} [32]. The vibrational bands for the Zr-OH-Zr and Hf-OH-Hf moiety[15] are centered at 530 cm^{-1} and 540 cm^{-1}, respectively.

The thermogravimetric analysis revealed the isolated crystalline materials lose surface-adsorbed and crystalline water molecules at 30-80 °C and 100-250 °C **fig. S8, Table S6**). The calculated number of molecules of lattice H_2O volatilized in the TGA experiments for Zr_2Re_6 and Hf_2Re_6 are respectively 9.54 and 8.44, per formula unit. Those values are close to 9, corresponding to the 6 metal-coordinated water and 3 lattice water molecules, observed in the single-crystal structure. A rapid weight loss step occurs around 350 °C, during which the materials lose more than 60% of their initial weight. PXRD analysis of post TGA samples suggested that at >400 °C, the material undergoes thermal decomposition to form tetragonal/monoclinic metal oxide of zirconium and hafnium, along with Re_2O_7 (**fig. S9**). Upon continued heating, Re_2O_7 vaporizes (vaporization temperature = 363 °C)[33], leaving behind either tetragonal zirconium oxide or monoclinic hafnium oxide (**fig. S10**).

SAXS characterization of the formation of Zr_2Re_6, Hf_2Re_6, Zr_2Tc_6 and Hf_2Tc_6 from Zr_4/Hf_4

Unlike the prior-reported sulphate-bridged Zr/Hf-dimers, the perrhenate/pertechnetate capped dimers are readily redissolved in water, despite solid-state neutrality. This provides opportunity to study (1) Solution speciation including similarities and differences between the four compositions, Zr_2Re_6, Hf_2Re_6, Zr_2Tc_6 and Hf_2Tc_6; and (2) The formation pathway, starting from the well-known flat-tetramer (**figure 1,** centre). Although the synthesis was initially carried out by dissolution/neutralization of Zr/Hf oxyhydroxide in perrhenic/pertechnic acid, employing the Zr/Hf oxychloride (Zr_4/Hf_4) as the M^{IV}-source provided a better understanding of the formation of the dimer, since Zr_4/Hf_4 solution speciation has been examined in prior studies, and it has a well-known solid-state structure.[2, 14, 34]

Prior studies[2, 35] describe the Zr_4/Hf_4 polyoxocation undergoing polymerization, including side-by-side linking of the flat tetramers. The current study agrees with this assessment based on the SAXS data under the relevant synthesis conditions (**figure 2**). Here, we have analysed the data of the $MOCl_2$ solutions to subsequently determine the effect of the added perrhenate/pertechnetate on Zr/Hf speciation. Also included in **figure 2** is simulated scattering for the flat tetramer. Visual comparison of this simulation to the experiment scattering confirms that the Zr_4/Hf_4 polyoxocations are undergoing polymerization, because the Guinier region (the curved elbow between q~0.3-0.6 $Å^{-1}$) of simulated M_4-scatttering is at higher-q than the experimental scattering curves (q~0.1-0.3 $Å^{-1}$). Both the $ZrOCl_2$ and $HfOCl_2$ scattering curves also exhibit a prominent structure factor; for example, the broad coulombic peak between q=0.06-0.5 $Å^{-1}$ (**figure 2**).

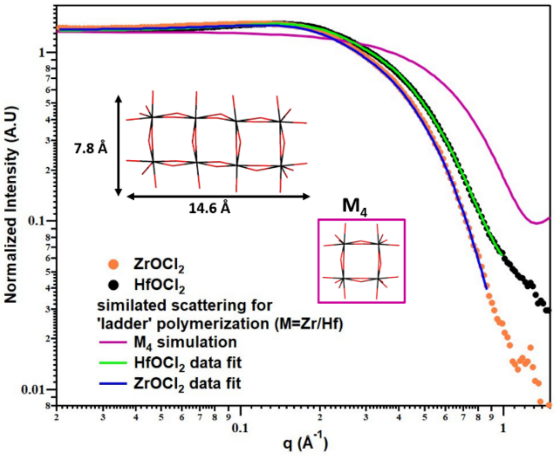

Figure 2. A) SAXS of 0.5 M $ZrOCl_2$ and $HfOCl_2$, intensity normalized for ease of comparison. (pH 0.48 and 0.61 respectively) plus the fits to these scattering curves (see **Table S9** and **figures S11 and S12** for fitting parameters). The form parameters for both scattering curves match that of a dimerized tetramer, an octamer (inset, 7.8×14.6 Å dimensions). Also presented is the simulated scattering for the flat tetramer (purple curve) showing the mismatch, due to polymerization of the tetramers in these solutions.

Due to this structure factor, determining the size, or R_g, via Guinier analysis or PDDF (R_g= radius of gyration, PDDF=pair distance distribution function) could not be reliably performed. This is also true for the SAXS of most of the heterometal solutions described in the following section. Instead, we fit the data to include both the form factor (size and shape) and structure factor (arrangement of scattering species in solution that produces the coulombic peak), and these parameters are summarized in **Table S9** and **fig. S11-S12**. The refined form parameters are similar for $ZrOCl_2$ and $HfOCl_2$ solutions, with dimensions of ~7.4×14.4 Å and 7.2×14.2 Å, respectively. This is most consistent with the simulated scattering and the dimension the hypothetical flat octamer (**figure 2,** inset). In addition, comparing the q-range of the experimental to the simulated scattering curves in the region of the spectra where the structure factor does not interfere (q>0.5 $Å^{-1}$, **figure S13**) also suggests this flat octamer could be the most abundant Zr/Hf polymer in these solutions. Also observed in **figure S13**, scattering of the $ZrOCl_2$ solution exhibits a greater difference between maximum and minimum intensity, as well as a better match in the high-q region (q>0.8 $Å^{-1}$) for simulated M_{10}, M_{12} and M_{16}. Both these features suggest the $ZrOCl_2$ solution exhibits more extensive polymerization than the $HfOCl_2$ solution, as well as greater polydispersity. The possible presence of flat hexamers along with the dominant octamers, given their similar simulated scattering curves (**figure S13**), suggests lability of the flat tetramer, since a putative flat hexamer would consist of a dimer plus a tetramer, requiring disassembly of the known, crystallized tetrameric form.

Next, we studied the Zr-Re, Hf-Re, Zr-Tc, and Hf-Tc reaction solutions by SAXS; the Tc analogues are shown in **figure 3**, and **figure S14** summarizes the Re-analogues. Redissolved crystals of $Zr^{IV}_2(OH)_2(Re^{VII}O_4)_6{\cdot}3H_2O$ and $Hf^{IV}_2(OH)_2(Re^{VII}O_4)_6{\cdot}3H_2O$ were likewise measured by SAXS. This was not practical for the Tc-analogues, because pertechnic acid crystallizes along with the dimer compounds, and it is difficult to extract pure Zr_2Tc_6/Hf_2Tc_6 from the mixture of colourless crystals. Select data were fit by a cylindrical form factor (**Table S10**, **fig. S15-S19**), consistent with the elongated shape of the dimer, regardless of how many perrhenate/pertechnetate are bound to the core dimer (discussed below). Note briefly, reaction solutions with higher Re:(Zr/Hf) ratios were not readily fit due to scattering interference from free perrhenate, discussed later. The Tc:Zr 1:1 and 3:1 ratio solutions exhibited a shallowing of the Guinier curve with increasing TcO_4^- (**figure 3**, q>0.2 $Å^{-1}$). With a 1:1 ratio of Tc:Zr, there is a good match to simulated scattering for a $Zr^{IV}_2(OH)_2(Tc^{VII}O_4)_4^{2+}$ (**figure 3A** inset) hypothetical derivative of the crystallized compound (**figure 3A)**.

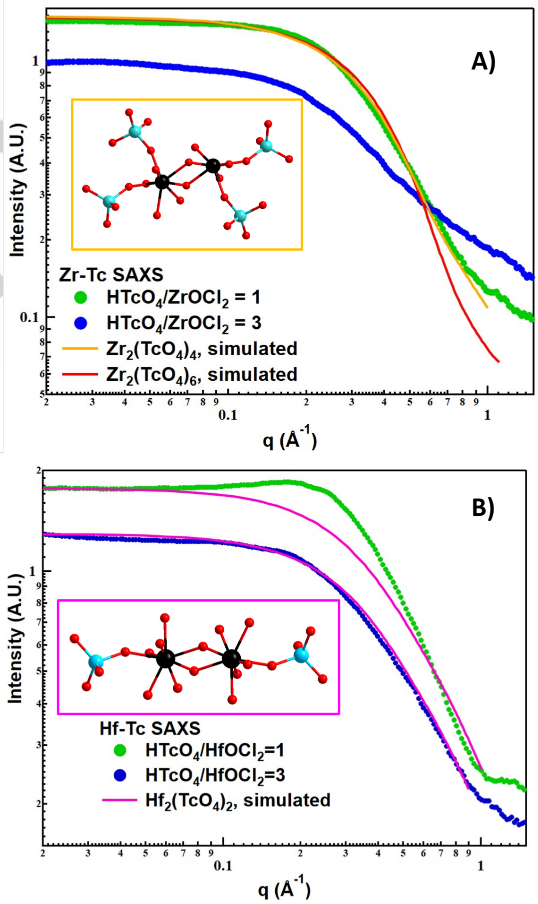

Figure 3. SAXS of $ZrOCl_2$-TcO_4^- **(A)** and $HfOCl_2$-TcO_4^- **(B)** reaction solutions compared to simulated scattering of the respective derivatives of the dimer compounds. For each M^{IV}, solution, concentrations are 0.25 M Zr-0.25 M Tc and 0.125 M Zr, 0.375 M Tc. See **Table S8** for full listing of concentrations and pH-values. The inset plus simulated scattering curves show the species for which the scattering best matches experimental scattering; $Zr^{IV}_2(OH)_2(Tc^{VII}O_4)_4^{2+}$ **(A)** and $Hf^{IV}_2(OH)_2(Tc^{VII}O_4)_2^{4+}$ **(B)**. $HTcO_4$/$HfOCl_2$=1 experimental scattering has a prominent structure factor that masks the Guinier region (see text for details).

The Tc:Hf 1:1 solution SAXS exhibits a prominent structure factor (the Coulombic peak between q~0.1-0.6 $Å^{-1}$), and it is therefore very different than any simulated scattering. However, both the Tc:Hf 1:1 and 3:1 scattering curves are most similar to simulated hypothetical $Hf^{IV}_2(OH)_2(Tc^{VII}O_4)_2^{4+}$ (**figure 3B**) derivative of the crystallized dimer. The 3:1 Tc:Hf ratio (the ratio of the isolated neutral product and the reaction solution from which it is obtained) does not exhibit the Coulombic peak, likely due to the lower Hf-concentration compared to the 1:1 solution (**Table S8**), and a corresponding decrease in concentration of the TcO_4-capped dimers. Coulombic peaks, or structure factors, represent organization of scattering species in solution, and are generally observed in high concentration solutions.

The 3:1 Tc:Zr SAXS differs from the analogous Hf-solution. Specifically, there is a rise in the scattering intensity at high-q (q>0.3 $Å^{-1}$), and lacks the structure factor. We attribute the former to free TcO_4^- in solution, discussed more extensively for rhenium analogues below. The latter could be related to the difference in charge of dominant species, as determined by SAXS: $Zr^{IV}_2(OH)_2(Tc^{VII}O_4)_4^{2+}$ vs. $Hf^{IV}_2(OH)_2(Tc^{VII}O_4)_2^{4+}$. The origin of structure factors is often described as repulsion between same-charged species. The proposed Hf-species is 4+ vs 2+ of the Zr-species, leading to greater repulsion and the corresponding structure factor.

The Re:Hf 1:1 SAXS (**fig. S14**) shows a good match to the hypothetical $Hf^{IV}_2(OH)_2(Re^{VII}O_4)_2^{4+}$ derivative species, and the 2:1 and 3:1 Re:Hf solutions show increasing scattering at high-q (q>0.3 $Å^{-1}$). The analogous Zr-ReO_4 solutions display an even higher rise in scattering at high-q with progressive increase in perrhenic acid. We also analysed perrhenic acid alone (**figure S14a**). This evidenced that the increased scattering at high-q with increased perrhenic acid addition to the Zr_4/Hf_4 solutions is due to free pehrrenate, or possibly small oligomers in solution, which is discussed more extensivley below (ESI-MS data). Scattering of redissolved $Hf^{IV}_2(OH)_2(Re^{VII}O_4)_6$ and $Zr^{IV}_2(OH)_2(Re^{VII}O_4)_6$ are nearly identical to their respective 2:1 Re:Zr/Hf solutions (**figure S14).**

To summarize the SAXS studies of the M-XO_4 reaction solutions and redissolved dimers; cationic derivitives with dissociated XO_4^-, rather than the complete neutral dimer, consistently appear to be more prevelant, whether we start with the reaction solution of different ratios, or the redissolved dimer-crystals. Second, Z (atomic number, commensurate with number of core electrons) of the studied metals very much affects the quality and ability to interpret the scattering data. For example, free perrhenate enhances the scattering at high-q significantly more than free pertechnetate, interfering with the dimer-scattering at lower-q. Similarly, the Zr-ReO_4 solution scattering displays more interference from free perrhenate than the Hf-ReO_4 solutions, due to the stronger scattering from the Hf_2-dimer core compared to the Zr_2-dimer. On the other hand, observing the free perrhenate scattering is important correlary evidence that cationic derivitives of the M_2X_6 dimers dominate these solutions. Regardless, the Zr-TcO_4, Hf-TcO_4 and Hf-ReO_4 solutions (and redissolved Re-analogue crystals) show good evidence for the presence of $Zr^{IV}_2(OH)_2(Tc^{VII}O_4)_4^{2+}$, $Hf^{IV}_2(OH)_2(Tc^{VII}O_4)_2^{4+}$ and $Hf^{IV}_2(OH)_2(Re^{VII}O_4)_2^{4+}$ as the dominant aqueous species.

ESI-MS characterization of aqueous Zr_2Re_6 and Hf_2Re_6

For further understanding of speciation in water, we also performed ESI-MS (both positive and negative ionization) analysis, with the caveat that that conditions for analysis are very different. Ideally, the SAXS experiments require 0.01-0.5 M, while ESI-MS require concentrations 100-1000× less. Four studied solutions that are discussed below are compiled in **figure S20**. Aqueous perrhenic acid solution alone shows formation of small anionic oligomers including monomers, dimers, trimers, tetramers, pentamers and hexamers of Re, and possible Re-oxidation states (due to the ionization process)[36] of III through VII (**figure S20B, S21, Table S11;**), similar to that recently identified in the mass spectrum of pyrazolium polyoxoperrhenate using laser ionization mass spectrometry.[37] The $ZrOCl_2$ aqueous solution exhibited no peaks in the negative ionization mode, and prior studies in the postive ionization mode identified Zr-polymers up to dodecamers.[38] In our prior ESI-MS study of $ZrOCl_2$ (postive mode), we identified species up to hexamers.[14] ESI MS (negative ionization) of the 3:1, 2:1 and 1:1 $HReO_4$:$ZrOCl_2$ reaction solutions identified the same Re-polymers (**figure S20A, S21, Table S11** for the 3:1 reaction solution), but in different ratios, compared to the $HReO_4$ solution.

Additional differences included a noisier baseline at higher m/z plus a new minor peak envelope at 2434.208 m/z with an isotope pattern attributable to a $Zr_2Re_{(7-9)}$ species. The noisy baseline arises from polydisperse polymerization in these low ionic strength solutions at higher pH (~3) than the typical reaction solutions (pH~1). However, dilute formic acid (**figure S20C**) simultaneously diminished the uninterpretable baseline and enhanced the peak at 2434.208 m/z, enabling easier interpretation. **Table S12** summarizes possible moiety formula based on peak positions and relative peak intensities within the envelope. Again, accounting for reduction of Re via the negative ionization process, one example formula is $[Zr_2(OH)_2(HRe^{V}O_3)_2(Re^{V}O_3)_7(H_2O)_6]^-$. An additional broad peak envelope is observed at 1124.2741m/z, and this is attributed to formate-capped Zr^{IV}-oxo hexamers[39] (**figure S22**), a common cluster topology for M^{IV}-polynuclear clusters and MOF nodes illustrated in **figure 1A** (M=Zr, Hf, Ce, Th, U, Np, Pu).[40]

UREX-type solvent extraction studies probing Zr-ReO_4 and Zr-TcO_4 co-extraction

Figure 4 gives an overview of the SAXS and SEM/EDS (scanning electron microscopy/energy dispersive spectroscopy) analysis of the solvent extraction of homometal ($ZrOCl_2$, $HReO_4$) and heterometal (Zr-$HReO_4$, Re:Zr ratios of 1, 2 and 3) species from nitric acid into TBP-kerosene, similar to procedures executed for SNF reprocessing.

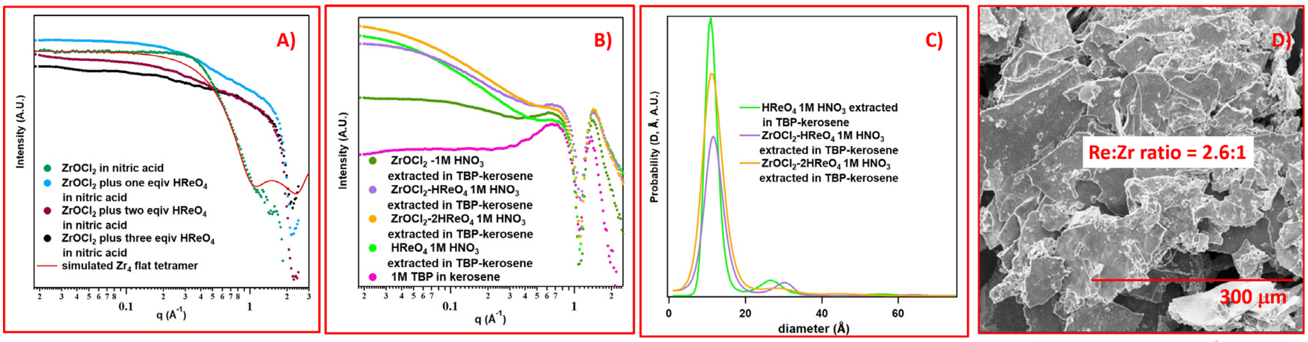

Figure 4. **A)** SAXS of Zr-HReO$_4$, ZrOCl$_2$ and HReO$_4$ solutions in 1M nitric acid. Concentrations of ZrOCl$_2$ and HReO$_4$ are the same as the SAXS studies in neat water (**Table S8**). **B)** SAXS of Zr-ReO$_4$, ZrOCl$_2$ and HReO$_4$ solutions extracted from 1M nitric acid into TBP-kerosene. **C)** Size distribution analysis of Zr-HReO$_4$ and HReO$_4$ solutions extracted from 1M nitric acid into TBP-kerosene. C) SEM image of extracted solid, isolated from TBP-kerosene (see also **figure S25).**

ZrOCl$_2$ (0.5M) in 1M nitric acid resembles the flat tetrameter (**figure 1**, center), by both comparing to simulated scattering, and a model fit that includes the structure factor (**figure S23, Table S9**). The acidic media appears to suppress the polymerization that is observed for both Zr and Hf in neat water. Addition of HReO$_4$ leads to flattering of the scattering curve, with the typical rise in scattering above q = 1 Å^{-1}, due to free HReO$_4$ in solution. With 1 equivalent of perrhenate, there is a rise in scattering and a shift of the Guinier elbow to lower q, suggesting formation of Zr-ReO$_4$ complexes and/or polymerization of perrhenate (discussed later). On the other hand, 2 and 3 equivalents of HReO$_4$ leads to weaker scattering, due to increased X-ray absorption, increased acidity that fragments metal-oxide polymers, and/or the decrease in Zr concentration (**Table S8**). Ultimately **Zr$_2$Re$_6$** (and **Hf$_2$Re$_6$**) can be crystallized from the HNO$_3$ solution with ~85% yield based on Zr/Hf, upon slow evaporation of reaction mixture for 7 days. This suggests that the perrhenate (pertechnetate) more favourably ligates M^{IV} than nitrate which would yield a 1d-polymer (**figure 1d**), despite the fact that nitrate is in large excess. SAXS of these same solutions extracted into TBP-kerosene are shown in **figure 4b**. The prominent peak at q~1.4 Å^{-1} in addition to the broad feature at q~0.7 Å^{-1} is attributed to TBP-kerosene, evidenced in the pink scattering curve of TBP-kerosene only. Extraction of ZrOCl$_2$ alone without perrhenic acid alters the scattering minimally above the solvent baseline, and it is not possible to provide accurate size analysis of this curve. On the other hand, extraction of ZrOCl$_2$-HReO$_4$ 1:1 and 2:1, and perrhenic acid alone exhibits meaningful scattering that was best fitted via a size distribution analysis with a form factor of a spherical aspect ratio of 2 (**figure S24**), and the probability distribution is shown in **figure 4c**. All three are similar in size with the main species exhibiting a diameter of 11 Å.

The intensity of peak centered at 11.0 Å increases with increasing Re:Zr ratio, and is largest for perrhenic acid alone, which might suggest that only perrhenic acid is extracted into TBP-kerosene, perhaps as the small oligomers observed in the ESI MS spectrum. However, semi-quantitative analysis of solids extracted from the 1:1 Re:Zr solution reveals that both Re and Zr are extracted with the 3:1 Re:Zr ratio exhibited in the Zr$_2$Re$_6$ dimer (**figures 4d & S25, Table S13**, experimental details in SI). Since these larger scattering species are not necessarily observed in the nitric acid solution, the nonpolar kerosene likely plays a role in promoting association by bonding or ion-pairing. The conflicting evidence between SAXS (suggesting extraction of Re only) and composition (suggesting co-extraction of Zr and Re) could again be due to the differential in scattering intensity of Re (Z=75) vs. Zr (Z=40), where scattering intensity scales by Z^2. For this reason, it was important to perform the analogous Zr-Tc extraction studies; Z(Tc)=43, nearly identical to Zr, thus removing this artifact.

Select analogous experiments of Zr-HTcO$_4$ (partially-limited by safety protocols) suggest HTcO$_4$ does increase extraction of Zr into TBP-kerosene from 1M nitric acid (**figure 5**). For the sake of consistency (and because a reasonable fit was obtained (**figure S26**), we used the same size distribution model for the HTcO$_4$ and Zr-HTcO$_4$ that was used for the Zr-HReO$_4$ analyses. Similarly, the major species has a diameter of 11.5 Å; but the Zr-HTcO$_4$ solution exhibits higher intensity scattering and concomitant higher size-distribution peak profile. This supports Zr-HTcO$_4$ coextraction by either bonding or ion-pairing, while ZrOCl$_2$ discussed prior (1M nitric acid, **figure 4B**) exhibits minimal extraction.

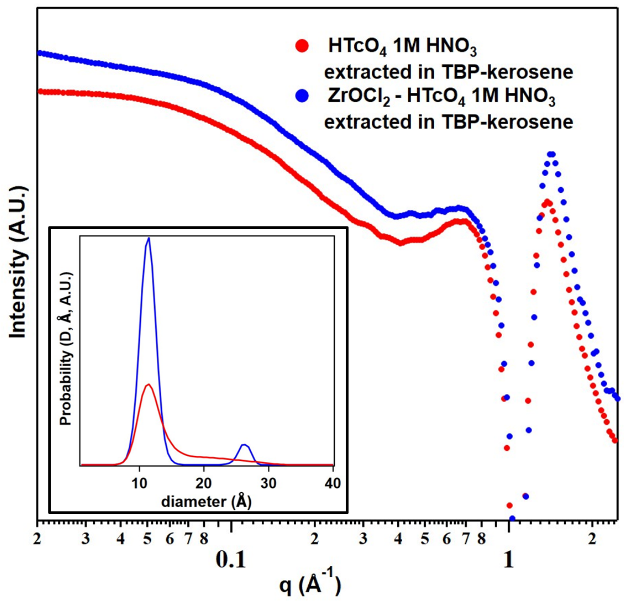

Figure 5. SAXS and size distribution analysis (inset) of HTcO$_4$ and Zr-HTcO$_4$ in 1M nitric acid, extracted into TBP-kerosene.

Due to instrument limitations, we could not analyze either the studied HNO$_3$ solutions or TBP-kerosene solutions by ESI-MS. Using acetonitrile as a representative organic solvent, we dissolved **Zr$_2$Re$_6$** (sparingly soluble) to investigate possible speciation of co-extracted $ZrOCl_2$-$HReO_4$ (and $ZrOCl_2$-$HTcO_4$ by inference). ESI-MS of acetonitrile with dissolved **Zr_2Re_6** reveals five signals below 1000m/z that are consistent with $[ReO_4]^-$, $[ReO_8H]^-$, $[Re_2O_9H_7]^-$, $[Re_3O_{11}]^-$, and $[Re_4O_{14}]^-$, and feature 5+, 6+, and 7+ Re oxidation states, where reduction occurs as part of the negative ionization process.[36] These oxoanions are the same as those described from the aqueous ESI MS (above) and also recently identified in the mass spectrum of pyrazolium polyoxorhenate.[37] In addition, several signals display mixed Zr/Re isotopic signatures. The major isotope of the most abundant Zr/Re species was observed at 1623.94 m/z with 60.72% abundance relative to the highest signal in the spectrum (**figure 6**).

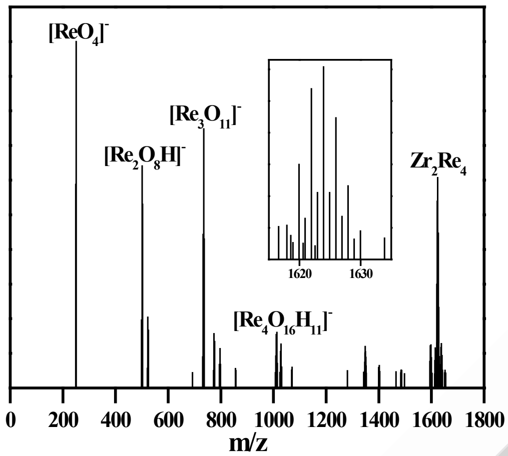

Figure 6. The experimental ESI-MS spectrum of Zr_2Re_6 in acetonitrile in the mass range of 0-1800m/z. Inset box shows an expansion of the Zr_2Re_4 peak centered at 1623.94 m/z.

Based on the distribution of intensities in the peak envelope, the Zr/Re nuclearity of the species was identified as Zr_2Re_4, and the inter-peak spacing of 1 m/z designated a -1 charge. Species of the general formula $[Zr_2(OH)_x(Re^{V}O_3)_y(Re^{VI}O_3)_z(Re^{VII}O_4)_u(H_2O)_v(CH_3CN)_w]^-$ (x=5-8; y=1-4; z=1-3; u=1-3) and are within 0.01% of the observed mass are summarized in **Tables S14** and **S15**. Similarly, smaller intensity peaks at 1637.92 m/z and 1651.91 m/z are matched respectively with $Zr_2Re_4^{1-}$ and $Zr_2Re_3^{1-}$, also summarized in **Tables S14** and **S15**.

Conclusion

To summarize, this study provides new knowledge about fundamental Zr/Hf aqueous speciation, as well as possible mechanisms of the Zr-TcO_4 co-extraction during nuclear fuel reprocessing, which involves direct bonding. Data supporting these hypotheses and the underlying fundamental knowledge include 1) single-crystal X-ray diffraction structures, 2) SAXS on all studied solutions including aqueous reaction solutions and solutions representing PUREX/UREX solvent extraction media; and 3) ESI-MS in water and acetonitrile (in lieu of TBP-kerosene).

Isolation of the Zr/Hf dimer as the four compositional analogues (**Zr_2Re_6**, **Hf_2Re_6**, **Zr_2Tc_6** and **Hf_2Tc_6**) along with SAXS studies suggests XO_4^- (X=Re, Tc) effectively cleaves aqueous $MOCl_2$-tetramers (M=Zr,Hf) and related oligomers. While polymerization of these simple aqueous Zr/Hf^{IV} tetramers has been proposed prior,[34c] disassembly of the tetramer building block into smaller units has not. Similar to our prior SAXS studies of Th-ReO_4 and Th-TcO_4 species,[24] TcO_4^- exhibits a trend of more extensive binding than ReO_4^- to Zr/Hf^{IV}.

SAXS of the TBP-kerosene extracted Zr-XO_4 (X=Re, Tc) produced ambiguous results, likely confounded by the stronger scattering of Re compared to Zr and Tc. Zr-ReO_4 SAXS studies indicated more favorable extraction of perrhenate polymers than Zr-ReO_4 species, but compositional analysis of Zr-ReO_4 extracted species suggests co-extraction in ratios similar to that presented in the **Zr_2Re_6** dimer-structure. On the other hand, SAXS studies confirmed more favorable co-extraction of Zr-TcO_4 than pertechnetate alone.

Future goals include unveiling additional compositions and topologies of the family of crystallized M^{IV}-XO_4 compounds including M=U, Np, Pu. Synthetic targets also include those with phosphonate ligands, to determine if and how they ligate M^{IV}-XO_4 compounds relevant to efficient nuclear fuel reprocessing.

Supporting Information

Supplementary information (SI) is available for this manuscript which contains details of synthesis and chemical characterization (SCXRD, SEM-EDS, FT-IR, PXRD, TGA and SAXS). Deposition numbers 2263497 (**Zr_2Re_6**), 2263498 (**Hf_2Re_6**), 2263499 (**Zr_2Tc_6**), and 2263500 (**Hf_2Tc_6**) contain the supplementary crystallographic data for this paper. These data are provided free of charge by the joint Cambridge Crystallographic Data Centre and Fachinformationszentrum Karlsruhe Access Structures service. The authors have cited additional references within the Supporting Information[24, 41].

Acknowledgements

There are no conflicts of interest to declare. This study was supported by the Department of Energy, National Nuclear Security Administration under Award DE-NA0003763. We acknowledge the Murdock Charitable Trust (Grant SR-2017297) for acquisition of the single-crystal X-ray diffractometer. The Tc-99 used in this research was supplied by the U.S. Department of Energy Isotope Program, managed by the Office of Isotope R&D and Production.

Keywords: Zirconium • Technetium • Nuclear Fuel • Hafnium •

References

[1] J. A. Sommers, L. Palys, N. P. Martin, D. B. Fast, M. Amiri and M. Nyman, *J Am Chem Soc* **2022**, *144*, 2816-2824.
[2] J. A. Sommers, D. C. Hutchison, N. P. Martin, L. Palys, J. M. Amador, D. A. Keszler and M. Nyman, *Inorg Chem* **2021**, *60*, 1631-1640.

[3] S. Jakobsen, D. Gianolio, D. S. Wragg, M. H. Nilsen, H. Emerich, S. Bordiga, C. Lamberti, U. Olsbye, M. Tilset and K. P. Lillerud, *Phys Rev B* **2012**, *86*, 125429.
[4] P. Ji, K. Manna, Z. Lin, A. Urban, F. X. Greene, G. Lan and W. Lin, *J Am Chem Soc* **2016**, *138*, 12234-12242.
[5] a) P. Ji, K. Manna, Z. Lin, X. Feng, A. Urban, Y. Song and W. Lin, *J Am Chem Soc* **2017**, *139*, 7004-7011; b) M. J. Cliffe, E. Castillo-Martínez, Y. Wu, J. Lee, A. C. Forse, F. C. N. Firth, P. Z. Moghadam, D. Fairen-Jimenez, M. W. Gaultois, J. A. Hill, O. V. Magdysyuk, B. Slater, A. L. Goodwin and C. P. Grey, *J Am Chem Soc* **2017**, *139*, 5397-5404.
[6] J. Winarta, B. Shan, S. M. McIntyre, L. Ye, C. Wang, J. Liu and B. Mu, *Cryst Growth Des* **2020**, *20*, 1347-1362.
[7] J. E. Mondloch, M. J. Katz, W. C. Isley Iii, P. Ghosh, P. Liao, W. Bury, G. W. Wagner, M. G. Hall, J. B. DeCoste, G. W. Peterson, R. Q. Snurr, C. J. Cramer, J. T. Hupp and O. K. Farha, *Nat Mater* **2015**, *14*, 512-516.
[8] a) R. J. Drout, K. Otake, A. J. Howarth, T. Islamoglu, L. Zhu, C. Xiao, S. Wang and O. K. Farha, *Chem Mater* **2018**, *30*, 1277-1284; b) M. Leloire, C. Walshe, P. Devaux, R. Giovine, S. Duval, T. Bousquet, S. Chibani, J.-F. Paul, A. Moissette, H. Vezin, P. Nerisson, L. Cantrel, C. Volkringer and T. Loiseau, *Chem Eur J* **2022**, *28*, e202104437.
[9] a) Z. Hu, A. Nalaparaju, Y. Peng, J. Jiang and D. Zhao, *Inorg Chem* **2016**, *55*, 1134-1141; b) L.-J. Li, P.-Q. Liao, C.-T. He, Y.-S. Wei, H.-L. Zhou, J.-M. Lin, X.-Y. Li and J.-P. Zhang, *J Mater Chem A* **2015**, *3*, 21849-21855.
[10] C. Wang, X. Liu, N. Keser Demir, J. P. Chen and K. Li, *Chem Soc Rev* **2016**, *45*, 5107-5134.
[11] a) H. G. T. Ly, G. Fu, A. Kondinski, B. Bueken, D. De Vos and T. N. Parac-Vogt, *J Am Chem Soc* **2018**, *140*, 6325-6335; b) A. Loosen, F. de Azambuja, S. Smolders, J. Moons, C. Simms, D. De Vos and T. N. Parac-Vogt, *Chem Sci* **2020**, *11*, 6662-6669.
[12] a) J. A. Sommers, L. Palys, N. P. Martin, D. B. Fast, M. Amiri and M. Nyman, *J Am Chem Soc* **2022**, *144*, 2816-2824; b) J. Moons, F. de Azambuja, J. Mihailovic, K. Kozma, K. Smiljanic, M. Amiri, T. Cirkovic Velickovic, M. Nyman and T. N. Parac-Vogt, *Angew Chem Int Ed* **2020**, *59*, 9094-9101; c) D. Van den Eynden, R. Pokratath, J. P. Mathew, E. Goossens, K. De Buysser and J. De Roo, *Chem Sci* **2023**, *14*, 573-585; d) D. Olynick, A. Schwartzberg and D. A. Keszler in *Chapter 10 - Mainstreaming inorganic metal-oxide resists for high-resolution lithography*, *Vol. 11* Eds.: A. Robinson and R. Lawson), Elsevier, **2016**, pp. 349-375.
[13] a) A. Clearfield and P. A. Vaughan, *Acta Crystallographica* **1956**, *9*, 555-558; b) T. V. Mit"kina, O. A. Gerasko, M. N. Sokolov, D. Y. Naumov and V. P. Fedin, *Russian Chem Bull* **2004**, *53*, 80-85.
[14] J. A. Sommers, D. C. Hutchison, N. P. Martin, K. Kozma, D. A. Keszler and M. Nyman, *J Am Chem Soc* **2019**, *141*, 16894-16902.
[15] Q. Sun, C. Liu, G. Zhang, J. Zhang, C.-H. Tung and Y. Wang, *Chem Eur J* **2018**, *24*, 14701-14706.
[16] P. J. Squattrito, P. R. Rudolf and A. Clearfield, *Inorg Chem* **1987**, *26*, 4240-4244.
[17] S. Øien-Ødegaard, C. Bazioti, E. A. Redekop, Ø. Prytz, K. P. Lillerud and U. Olsbye, *Angew Chem Int Ed* **2020**, *59*, 21397-21402.
[18] a) K. Kozma, L. N. Zakharov and M. Nyman, *Cryst Growth Des* **2020**, *20*, 6519-6527; b) S. Goberna-Ferron, D. H. Park, J. M. Amador, D. A. Keszler and M. Nyman, *Angew Chem Int Edit* **2016**, *55*, 6221-6224.
[19] P. Bénard-Rocherullé, J. Rius and D. Louër, *J Solid State Chem* **1997**, *128*, 295-304.
[20] Y. Zhang, F. de Azambuja and T. N. Parac-Vogt, *Coord Chem Rev* **2021**, *438*, 213886.
[21] a) J. Garraway and P. D. Wilson, *J Less-common metals* **1985**, *106*, 183-192; b) K. George, A. J. Masters, F. R. Livens, M. J. Sarsfield, R. J. Taylor and C. A. Sharrad, *Hydrometallurgy* **2022**, *211*, 105892.
[22] a) E. Boros and A. B. Packard, *Chem Rev* **2019**, *119*, 870-901; b) J. R. Dilworth and S. I. Pascu, *ChemSoc Rev* **2018**, *47*, 2554-2571.
[23] a) M. J. Sarsfield, A. D. Sutton, I. May, G. H. John, C. Sharrad and M. Helliwell, *Chem Comm* **2004**, 2320-2321; b) A. D. Sutton, I. May, C. A. Sharrad, M. J. Sarsfield and M. Helliwell, *Dalton Transac* **2006**, 5734-5742; c) A. D. Sutton, G. H. John, M. J. Sarsfield, J. C. Renshaw, I. May, L. R. Martin, A. J. Selvage, D. Collison and M. Helliwell, *Inorg Chem* **2004**, *43*, 5480-5482.
[24] M. Shohel, J. Bustos, G. D. Stroscio, A. Sarkar and M. Nyman, *Inorg Chem* **2023**, *62*, 10450-10460.
[25] E. A. Puzikov, B. Y. Zilberman, Y. S. Fedorov, I. V. Blazheva, A. P. Krinitsyn, L. V. Sytnik, D. V. Ryabkov and N. D. Goletskii, *Radiochem* **2015**, *57*, 273-284.
[26] J. D. Law in *Aqueous Reprocessing of Used Nuclear Fuel*, **2018**, pp. 1-26.
[27] R. Bhattacharjee, E. T. Hare and P. Miro, *Inorg Chem* **2023**, *62*, 5081-5087.
[28] a) D. B. McWhan and G. Lundgren, *Inorg Chem* **1966**, *5*, 284-289; b) D. L. Rogachev, A. S. Antsyshkina and M. A. Porai-Koshits, *J Struct Chem* **1972**, *13*, 239-243.
[29] D. W. Wester, *Inorg Chem* **1982**, *21*, 3382-3385.
[30] K. E. Knope and L. Soderholm, *Chem Rev* **2013**, *113*, 944-994.
[31] R. D. Aines and G. R. Rossman, *J Geophys Res: Solid Earth* **1984**, *89*, 4059-4071.
[32] a) M.-M. Li, J.-W. Cao, X.-L. Qin, X.-Y. Liu, X.-Q. Yuan, X.-T. Dong, Q. Guo, Y. Sun and P. Zhang, *ACS Omega* **2022**, *7*, 5437-5441; b) R. H. Busey and O. L. Keller, *The J Chem Phys* **1964**, *41*, 215-225.
[33] J. G. Darab and P. A. Smith, *Chem Mater* **1996**, *8*, 1004-1021.
[34] a) R. E. Ruther, B. M. Baker, J.-H. Son, W. H. Casey and M. Nyman, *Inorg Chem* **2014**, *53*, 4234-4242; b) Y.-J. Hu, K. E. Knope, S. Skanthakumar, M. G. Kanatzidis, J. F. Mitchell and L. Soderholm, *J Am Chem Soc* **2013**, *135*, 14240-14248; c) A. Singhal, L. M. Toth, J. S. Lin and K. Affholter, *J Am Chem Soc* **1996**, *118*, 11529-11534.
[35] M. Bremholm, H. Birkedal, B. B. Iversen and J. S. Pedersen, *J Phys Chem C* **2015**, *119*, 12660-12667.
[36] S. Banerjee and S. Mazumdar, *Int J Anal Chem* **2012**, *2012*.
[37] M. A. Volkov, A. P. Novikov, N. E. Borisova, M. S. Grigoriev and K. E. German, *Inorg Chem* **2023**, *62*, 13485-13494.
[38] T. Sasaki, O. Nakaoka, R. Arakawa, T. Kobayashi, I. Takagi and H. Moriyama, *J Nucl Sci Technol* **2010**, *47*, 1211-1218.
[39] J. I. Choi, H. Chun and M. S. Lah, *J Am Chem Soc* **2018**, *140*, 10915-10920.
[40] A. M. Hastings, M. Fairley, M. C. Wasson, D. Campisi, A. Sarkar, Z. C. Emory, K. Brunson, D. B. Fast, T. Islamoglu, M. Nyman, P. C. Burns, L. Gagliardi, O. K. Farha, A. E. Hixon and J. A. LaVerne, *Chem Mater* **2022**.
[41] a) Bruker AXS, M. SAINT Plus Version 8.34a, WI2013; b) S. G. M. Sheldrick, Bruker-Siemens area Detector. Absorb. other Correct. Version 2008/12008; c) G. Sheldrick, *Acta Cryst A* **2015**, *71*, 3-8; d) G. Sheldrick, *Acta Cryst A* **2008**, *64*, 112-122; e) O. V. Dolomanov, L. J. Bourhis, R. J. Gildea, J. A. K. Howard and H. Puschmann, *J Appl Cryst* **2009**, *42*, 339-341; f) J. Ilavsky and P. R. Jemian, *J Appl Cryst* **2009**, *42*, 347-353; g) X. Zuo, G. Cui, K. M. Merz, L. Zhang, F. D. Lewis and D. M. Tiede, *PNAS* **2006**, *103*, 3534-3539; h) G. Beaucage, *J Appl Cryst* **1995**, *28*, 717-728.

Entry for the Table of ContentS

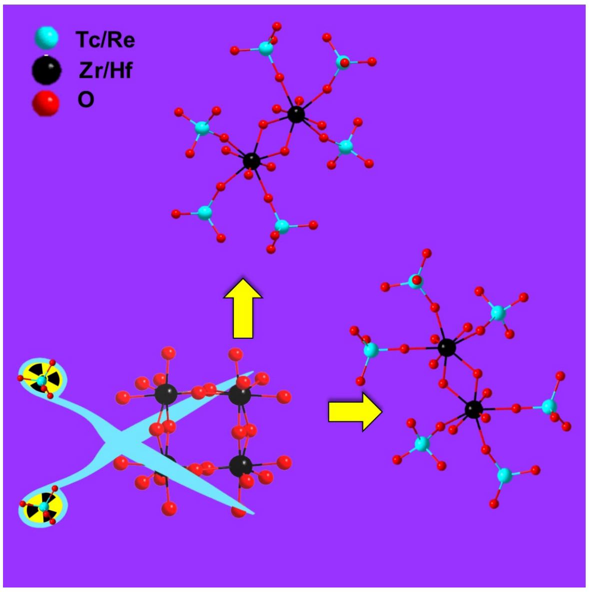

The well-known Zr/Hf_4-tetramer is cleaved in aqueous solutions by perrhenate/pertechnetate to yield a dihydroxide dimer capped by these oxoanions. Structure and solution characterization of this complex along with solvent extraction studies elucidates ^{93}Zr-^{99}Tc co-extraction (two of the most abundant and problematic ^{235}U fission products) during nuclear fuel reprocessing.

Institute and/or researcher Twitter usernames: @NymanMay, @shohel_Md_, @jenn_chem_